

NUMERICAL PREDICTION OF THE RESPONSE OF A SQUAT SHEAR WALL SUBJECTED TO MONOTONIC LOADING THROUGH PARC_CL MODEL

B. BELLETTI[†], R. ESPOSITO[#] AND C. DAMONI*

[†] University of Parma
Parco Area delle Scienze 181/A, 43124 Parma, Italy
e-mail: beatrice.belletti@unipr.it

[#] Delft University of Technology
Faculty of Civil Engineering and Geosciences, Stevinweg 1, 2628 CN, Delft, The Netherlands
E-mail: R.Esposito@tudelft.nl

* University of Parma
Parco Area delle Scienze 181/A, 43124 Parma, Italy
e-mail: cecilia.damoni@nemo.unipr.it

Key words: squat shear wall, shear resistance, nonlinear finite element analyses, constitutive model

Abstract: The paper adopts the FEM to describe the behaviour of a squat shear wall subjected to monotonic loading conditions. Nonlinear finite element analyses (NLFEA) have been performed with the model, denoted as PARC_CL, implemented at the University of Parma in the user's subroutine UMAT.for for the ABAQUS Code. The PARC_CL model, suitable for loading-unloading-reloading conditions, is an evolution of the PARC model. The new model provides a more accurate response prediction for reinforced concrete structures subjected to monotonic loading, but characterized by internal stress redistribution and/or cracks opening and closing phenomena.

The PARC_CL model has been adopted to simulate the response of a squat shear wall whose experimental results have been presented at the last Concrack2 Benchmark Workshop. The obtained results have been compared with the results of NLFEA carried out with DIANA code in order to focus on the main differences detected in the structural response of a shear-critical structure analyzed with a standard code or with a crack model tailored on shear critical structure analyses. Finally the design shear capacity of the wall has been determined analytically and with PARC_CL and DIANA models applying the safety format methods for NLFEA.

1. INTRODUCTION

In the current paper the behavior of a squat shear wall subjected to monotonic loading is investigated by means of NLFEA. The results obtained are compared to the experimental results provided by CEOS.fr [1] and presented during the last Concrack2 Benchmark Workshop [2]. The squat shear wall has been

analyzed with the PARC_CL model [3], [4], implemented at the University of Parma in the user's subroutine UMAT.for for ABAQUS code [5]. PARC_CL model is an evolution of the PARC model [6]. PARC_CL model is a total strain fixed crack model that describes the behavior up to failure of reinforced concrete structures subjected to loading-unloading-reloading conditions. The model is

tailored to analyze structures failing in shear. The concrete and steel behavior as well as their interaction phenomena are therefore modeled with appropriate constitutive laws. In particular the aggregate interlock effect, the tension stiffening effect and the dowel action effect are implemented in the stiffness matrix of the model on the basis of proven relations available in literature. The new version of PARC model (PARC_CL model) provides a more accurate prediction of reinforced concrete structures subjected to monotonic loading, but characterized by internal stress redistribution and/or cracks opening and closing phenomena [6], [7]. The PARC_CL model can also be useful for cyclic loading, even though hysteretic loops and plastic strains cannot be properly considered in the current version of the model due to secant unloading implementation. Future researches will deepen the modeling under loading-unloading-reloading conditions.

The results obtained with PARC_CL model have been compared with those one obtained with the standard code DIANA [8], [9]. The aim of the comparison is to focus on the main differences detected in the structural prediction obtained with a commercial software (DIANA), used in the civil engineering practice, and with a specific crack model (PARC_CL), mostly used in the research field, focused on the investigation of the concrete-to-concrete and concrete-to-reinforcement interface behavior. As a matter of fact some relations used in the crack model implemented in DIANA are more simple and for wider use than the relations used in PARC_CL model; the aspects strictly related to shear-failure are in fact treated in the two software with different levels of refinement.

Furthermore the design shear capacity of the squat shear wall has been evaluated following the prescriptions of the new Model Code 2010 (MC2010) [10] that proposes different analytical and numerical calculation methods for the evaluation of the design shear capacity of slender and squat elements.

For slender elements the MC2010 proposes to evaluate the design shear capacity according to four levels of approximation: Level I, II and

III refer to analytical calculation methods while Level IV refers to numerical methods, performed with NLFEA. Within Level IV the results obtained from NLFEA are properly reduced, in order to obtain the same safety level of analytical calculations, according to three different safety format methods denoted as Partial Factor method (PF), Global Resistance Factor method (GRF) and Estimation of Coefficient of Variation of resistance method (ECOV). Further details of the safety format methods are given in [9], [10].

For squat elements the design shear capacity can be evaluated analytically with a strut and tie model.

In this paper the design shear capacity of the squat wall has been evaluated analytically, with a strut and tie model, and numerically, applying the prescriptions of Level IV approximation, comparing the design shear capacity obtained with PARC_CL and DIANA models.

The application of the MC2010 prescriptions for the evaluation of the design shear capacity is to underline the power of NLFEA in the structural assessment, useful for both designer and researchers in civil engineering.

2. CASE STUDY

The squat shear wall analyzed in this paper was tested by CEOS.fr [1] and the experimental results presented in [2]. The experimental program aimed to investigate some aspects related to the control of cracking in reinforced concrete structures through the modeling of the behavior of tested monotonic and cycling loading.



Figure 1: Experimental set-up.

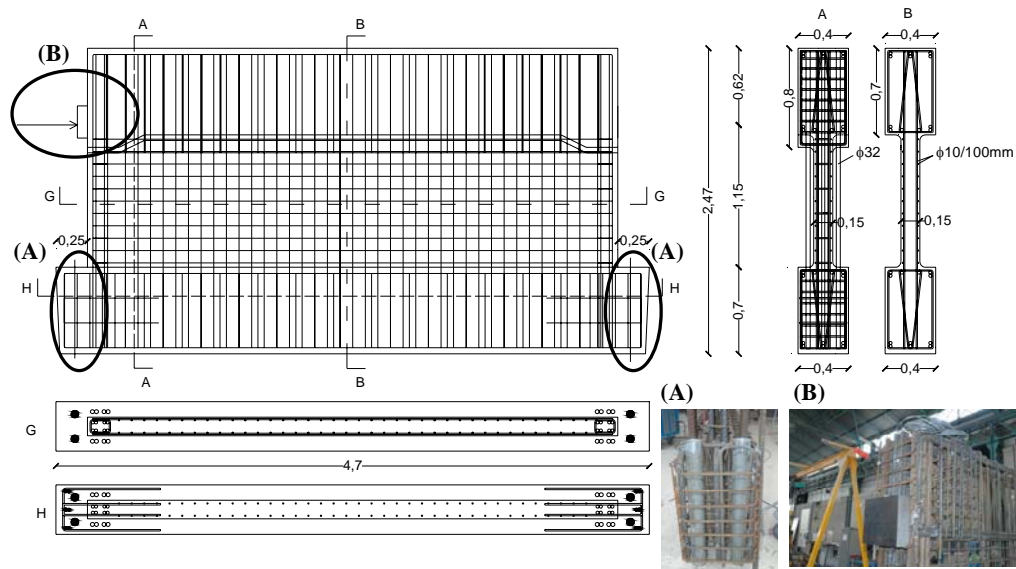


Figure 2: Reinforcement layout and boundary conditions (dimension in m).

In this section the main indications of the experimental set-up of the wall are given. The squat shear wall was clamped at the top and at the bottom in two highly reinforced beams and the left and right extremities were seamed with rebars. The wall was placed in a rigid metallic frame and subjected to monotonic loading-unloading through two jacks placed at the top of the wall, Figure 1. Several sensors were placed on the two faces of the wall in order to measure the crack width and the strain in rebars. In Table 1 the mean mechanical properties of concrete and steel, measured during the experimental test, are reported.

Table 1: Mean mechanical properties of concrete and steel measured during the test.

Concrete		Steel	
f_c [N/mm ²]	-42.5	f_v [N/mm ²]	554
f_t [N/mm ²]	3.3	E_s [N/mm ²]	189274
E_c [N/mm ²]	22060	f_u [N/mm ²]	634
ν	0.19		

Figure 2 shows the reinforcement layout and the boundary conditions of the wall. The wall is 4.7m long and 2.47m high. The web panel is 4.2m x 1.15m. The main reinforcement grid is made of $\phi 10/100$ mm and it is placed in the web panel. Further reinforcing bars were placed in the wall flanges and at the wall extremities, in order to prevent premature local

failure of the wall during the test. During the experimental test the wall failed under the loading plate for crushing of concrete. The reinforcement didn't yield up to failure. The maximum load value measured during the test was $P_{u,exp}=4710$ KN.

3 PARC_CL MODEL

The PARC_CL model [3], [4] which is the evolution of PARC model [6], describes the behavior up to failure of reinforced concrete structures subjected to loading-unloading-reloading conditions. The concrete and steel behavior as well as their interaction phenomena are taken into account.

PARC_CL model is a total strain fixed crack model. When the maximum tensile principal stress reaches the concrete tensile strength, cracking starts to develop and the 1,2 coordinate system is fixed. The smeared reinforcement approach is adopted, so the angle between the direction of the i -th order of bar and the 1-direction is equal to $\alpha_i = \theta_i - \psi$, being ψ the angle between the 1-direction and local element x -direction, and θ_i is the angle between the direction of the i -th order of bar and the x -direction. The concrete behavior is modeled taking into account the effect of multi-axial state of stress on concrete strength,

residual tensile stresses and aggregate interlock phenomena.

The reinforcement behavior is modeled with an elasto-plastic with hardening law by considering also dowel action and tension stiffening phenomena.

The total strains at each integration point are calculated, in the $1,2$ coordinate system, as the sum of the elastic (superscript el) and the inelastic (superscript cr) strains (Figure 3(b)):

$$\varepsilon_1 = \varepsilon_1^{el} + \varepsilon_1^{cr} = \varepsilon_1^{el} + w/a_m \quad (1)$$

$$\varepsilon_2 = \varepsilon_2^{cr} \quad (2)$$

$$\gamma_{12} = \gamma_{12}^{el} + \gamma_{12}^{cr} = \gamma_{12}^{el} + v/a_m \quad (3)$$

where w is the crack width, v is the crack sliding and a_m is the crack spacing, depending on the transmission length of bond between concrete and steel [7]. The strains in the x,y coordinate system, $\{\varepsilon^{(x,y)}\}$, are obtained through the transformation matrix $[T_\varepsilon]$, which is a function of the fixed angle ψ .

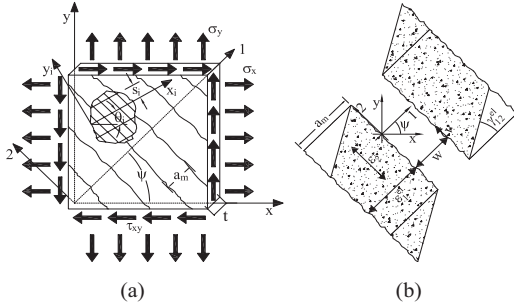


Figure 3: (a) Reinforced concrete membrane element subjected to plane stress state; (b) kinematic quantities.

The stiffness matrix in the x,y coordinate system, $[D(x,y)]$, is given in Eq. (4):

$$\begin{aligned} [D^{(x,y)}] &= [T_\varepsilon]^T [D_c^{(1,2)}] [T_\varepsilon] + [T_\theta]^T [D_s^{(x,y_i)}] [T_\theta] = \\ &= [T_\varepsilon]^T \begin{bmatrix} \bar{E}_{c1} & 0 & 0 \\ 0 & \bar{E}_{c2} & 0 \\ 0 & 0 & \beta G \end{bmatrix} [T_\varepsilon] + \\ &+ [T_\theta]^T \begin{bmatrix} \rho_t \bar{E}_{si} g_i & 0 \\ 0 & \rho_t d_i \end{bmatrix} [T_\theta] \end{aligned} \quad (4)$$

The concrete stiffness matrix $[D_c^{(1,2)}]$ is defined as a function of concrete constitutive model in tension and in compression (\bar{E}_{c1} and \bar{E}_{c2}) and of the aggregate interlock effect (βG).

The steel stiffness matrix $[D_s^{(x_i,y_i)}]$ is defined, in the x_i,y_i coordinate system, as a function of a reinforcement constitutive model (\bar{E}_{si}), tension stiffening (g_i) and dowel action (d_i). The transformation matrixes $[T_\varepsilon]$ and $[T_\theta]$ are used to rotate the concrete matrix from the $1,2$ to the x,y coordinate system and the steel matrix from the x_i,y_i to the x,y coordinate system, respectively.

Secondary cracking, perpendicular to primary cracking, is considered by imposing \bar{E}_{c2} equal to zero.

3.1 Constitutive model for concrete and steel

The stress-strain relationship for concrete is described with Eq. (5) and Eq. (6) for concrete in tension and compression, respectively, Figure 4.

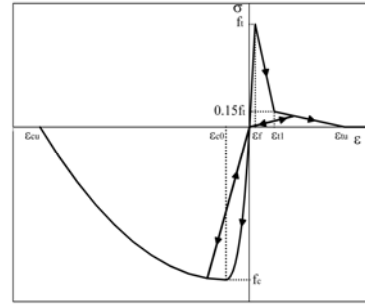


Figure 4: Constitutive model for concrete.

$$\sigma = \begin{cases} E_c \varepsilon & 0 \leq \varepsilon < \varepsilon_f \\ f_{ct} \left[1 + 0.85 (\varepsilon - \varepsilon_f) / (\varepsilon_f - \varepsilon_{t1}) \right] & \varepsilon_f \leq \varepsilon < \varepsilon_{t1} \\ 0.15 f_{ct} \left[1 + (\varepsilon - \varepsilon_{t1}) / (\varepsilon_{t1} - \varepsilon_{tu}) \right] & \varepsilon_{t1} \leq \varepsilon < \varepsilon_{tu} \end{cases} \quad (5)$$

$$\sigma = \begin{cases} \frac{E_c/E_{cs} - \varepsilon/\varepsilon_{c0}}{1 + (E_c/E_{cs} - 2)\varepsilon/\varepsilon_{c0}} E_{cs} \varepsilon & \varepsilon_{c0} \leq \varepsilon < 0 \\ f_c \left[1 - (\varepsilon - \varepsilon_{c0})^2 / (\varepsilon_{cu} - \varepsilon_{c0})^2 \right] & \varepsilon_{cu} \leq \varepsilon < \varepsilon_{c0} \end{cases} \quad (6)$$

where E_c and E_{cs} are the initial modulus of elasticity and the secant stiffness corresponding to the peak strain ε_{c0} , respectively.

The stress-strain relationship for concrete in tension is defined as a function of its tensile strength f_{ct} , the concrete strain at cracking ε_f , the strain ε_{t1} and ε_{tu} (corresponding to residual stress equal to $0.15 f_{ct}$ and zero, respectively):

$$\varepsilon_{t1} = 0.15\varepsilon_f + G_f (2 - 0.15\alpha_f) / a_m f_{ct} \quad (7)$$

$$\varepsilon_{tu} = \alpha_f G_f / a_m f_{ct} \quad (8)$$

where G_f is the fracture energy in tension.

The compressive branch before reaching the peak is defined in agreement with Sargin's relation and after the peak with Feenstra's relation [11] as a function of the concrete compressive strength f_c and concrete fracture energy in compression G_{fc} assumed equal to $250 G_f$ [12]. Therefore the ultimate concrete strain in compression is given by Eq. (9):

$$\varepsilon_{cu} = \varepsilon_{c0} + 3G_{fc} / 2 a_m f_c \quad (9)$$

Multi-axial stress state is considered by reducing the compressive strength and the corresponding peak strain due to lateral cracking [13], as given in Eq. (10):

$$\zeta = 1 / (0.85 - 0.27 \varepsilon_t / \varepsilon_{c0}) \quad (10)$$

being ε_t the tensile strain.

An elastic-plastic with hardening relation has been used for steel, Eq. (11).

$$\bar{E}_{si} = \begin{cases} E_{si} & \varepsilon_{si} \leq \varepsilon_{syi} \\ [f_{syi} + (\varepsilon_{si} - \varepsilon_{syi}) E_{spi}] / \varepsilon_{si} & \varepsilon_{syi} \leq \varepsilon_{si} < \varepsilon_{sli} \\ f_{sui} / \varepsilon_{si} & \varepsilon_{sli} \leq \varepsilon_{si} < \varepsilon_{ui} \end{cases} \quad (11)$$

Being, for each i -th rebar, E_{si} the elastic Young modulus; E_{spi} hardening modulus; ε_{syi} and f_{syi} the yielding strain and stress, ε_{sli} ε_{sli} the strain corresponding to the beginning of hardening and ε_{ui} the ultimate strain corresponding to the ultimate strength f_{sui} .

3.2 Aggregate interlock

The aggregate interlock effect is evaluated on the basis of the crack width, w , and the crack sliding, v [14]:

$$\tau_{12} = \bar{\tau} \left(1 - \sqrt{\frac{2w}{D_{max}}} \right) \frac{a_3 + a_4 |v/w|^3}{1 + a_4 (v/w)^4} \frac{1}{w} v \quad (12)$$

where $\bar{\tau} = 0.27 f_c$; $a_3 = 2.45/\bar{\tau}$; $a_4 = 2.44(1 - 4/\bar{\tau})$, D_{max} is the maximum aggregate diameter.

Aggregate interlock relation can be schematized with a bilinear curve (Figure 5) in which the endpoint of the elastic part A(v^* , τ^*) has coordinates given by Eq. (13)-(14):

$$v^* = f_c w / a_5 + a_6 \quad (13)$$

$$\tau^* = \bar{\tau} \left(1 - \sqrt{\frac{2w}{D_{max}}} \right) \frac{a_3 + a_4 |v^*/w|^3}{1 + a_4 (v^*/w)^4} \frac{1}{w} v^* = c^* v^* \quad (14)$$

where $a_5 = 0.366 f_c + 3.333$ and $a_6 = f_c / 110$.

The proposed bilinear curve is used to define the stress-strain relationship between the shear stress τ_{12} and the shear strain γ_{12}^{cr} in the cracked phase of the concrete. In this phase the tangential elastic modulus, G_{cr} , is equal to:

$$G_{cr} = \begin{cases} G_{cr}^* = c^* a_m & \gamma_{12}^{cr} < \gamma_{cr}^* \\ \tau^* / \gamma_{12}^{cr} & \gamma_{12}^{cr} \geq \gamma_{cr}^* \end{cases} \quad (15)$$

where c^* is defined with Eq. (14) and $\gamma_{cr}^* = v^* / a_m$.

The shear modulus is defined by multiplying its initial values for the shear retention factor β (Figure 5), given in Eq. (16):

$$\beta = \begin{cases} 1 & \text{uncracked phase } \gamma_{12} \leq \gamma_f \\ G_{cr} / (G_{cr} + G) & \text{cracked phase } \gamma_{12} > \gamma_f \end{cases} = \begin{cases} 1 & \gamma_{12} \leq \gamma_f \\ G_{cr}^* / (G_{cr}^* + G) & \gamma_f < \gamma_{12} < \gamma_p \\ \tau^* / G \gamma_{12} & \gamma_{12} \geq \gamma_p \end{cases} \quad (16)$$

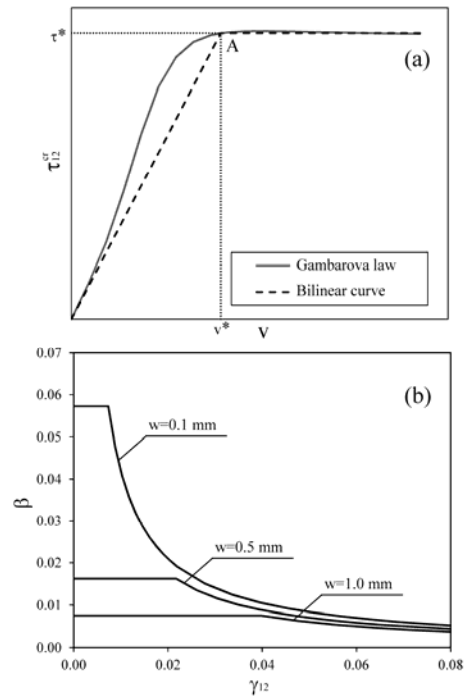


Figure 5: Aggregate interlock model: (a) shear stress-slip relationship, (b) shear retention factor for different crack width values.

being G and G_{cr} the initial and degraded values of the shear modulus, respectively. The strain γ_f corresponds to the shear strain at the onset of concrete cracking. The strain γ_p defines the point after which the shear stress remains constant for a given crack width w , Eq. (17):

$$\gamma_p = \gamma_{cr}^* + \tau^*/G \quad (17)$$

The coefficient β is assumed to be constant when unloading occurs.

The aggregate interlock phenomenon is neglected for crack width values higher than half of the maximum aggregate diameter.

3.3 Tension stiffening

In the PARC_CL model both the stress σ_{si}^* in the i -th steel bar near the cracks and the stress σ_{si} far from the cracks are taken into account. It is well known that the relationship between the two steel stresses defined above is governed by the tension stiffening effect. In the proposed model, the stress σ_{si}^* is evaluated by means of an appropriate increment of the steel bar average strain, as suggest by Giuriani [15], and it is evaluated with the following equations (Figure 6):

$$\begin{aligned} \sigma_{si}^* &= \bar{E}_{si} (\varepsilon_{si} + \Delta\varepsilon_{si}) \\ &= \bar{E}_{si} \left(1 + \frac{\Delta\varepsilon_{si}}{\varepsilon_{si}} \right) \varepsilon_{si} = \bar{E}_{si} g_i \varepsilon_{si} \end{aligned} \quad (18)$$

where:

$$\Delta\varepsilon_{si} = \varepsilon_{si}^* g_i \quad (19)$$

$$\varepsilon_{si}^* = (w \cos^2 \alpha_i + v \sin \alpha_i \cos \alpha_i) / a_m \quad (20)$$

$$g_i = g_{li} + k_1 g_{2i} (\varepsilon_{si}^*)^{k_2 - 1} \quad (21)$$

with:

$$g_{li} = \lambda_i \frac{\cosh \lambda_i - 1}{\sinh \lambda_i}$$

$$g_{2i} = \frac{2 \tau_0}{\tau_1 a_m} \lambda_i \frac{\cosh \lambda_i - 1}{\sinh \lambda_i}$$

$$\lambda_i = \sqrt{\frac{\tau_1 a_m^2}{0.5 E_{si} \phi_i}}$$

$$\tau_0 = 3 \text{ MPa}; \quad \tau_1 \phi_i = 75 \text{ MPa};$$

$$k_1 = 4.0; \quad k_2 = 0.2$$

The g_i coefficient could theoretically reach infinite values for steel strain values that

vanish but, in order to respect the physical reality, the maximum value of g_i coefficient is limited to $g_{i,lim}$, defined by Eq. (22):

$$g_{i,lim} = g_{li} + k_1 g_{2i} (\varepsilon_{cr})^{k_2 - 1} \quad (22)$$

where ε_{cr} is the concrete strain at the first appearance of cracks.

In unloading condition the coefficient g_i is assumed constant (Figure 6).

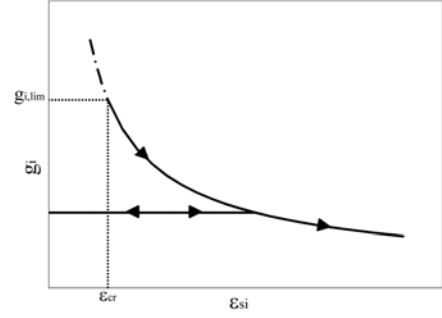


Figure 6: Variation of coefficient g_i as a function of the strain in the ε_{si} steel bar .

3.4 Dowel action

In the smeared crack approach perspective, the dowel action effect is considered trough the evaluation of a shear stress perpendicular to i -th bar direction τ_{Sdi} , by adopting the formulation proposed by Walraven and Reinhardt [16], Eq. (23):

$$\tau_{Sdi} = \frac{13.66 \rho f_c^{0.38}}{\phi_i^{0.25} \eta^{0.64} (\delta + 0.2)} s_i \gamma_{si} = d_i \gamma_{si} \quad (23)$$

where γ_{si} is the transversal strain of the steel bar evaluated in x_i, y_i coordinate system, given by Eq. (24):

$$\gamma_{si} = -2 \cos \alpha_i \sin \alpha_i \varepsilon_1 + (\cos^2 \alpha_i - \sin^2 \alpha_i) \gamma_{12} \quad (24)$$

being δ and η the bar deformations parallel and perpendicular respectively to the i -th directions of reinforcing bar, Eq. (25)-(26):

$$\delta = \varepsilon_{si} a_m / \cos \alpha_i \quad (25)$$

$$\eta = \gamma_{si} a_m / \cos \alpha_i \quad (26)$$

In Figure 7 the stress τ_{Sdi} versus the strains γ_{si} curves are shown for different values of longitudinal strain ε_{si} of steel bar in the i -th direction. A secant unloading conditions is considered (Figure 7).

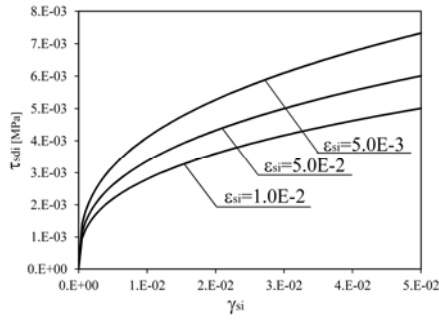


Figure 7: Dowel action model.

4 EVALUATION OF THE DESIGN SHEAR CAPACITY WITH NLFEA

In this sections the FEM used to carry out the analyses with PARC_CL model is described. The main results obtained with PARC_CL model are shown and compared to the results obtained with the standard code DIANA and with the experimental results. In particular the load-deflection curves, the load-crack width curve and the crack pattern evolution are reported. Furthermore the safety format methods proposed by the MC 2010 [10] have been applied to the results obtained by NLFEA in order to obtain the design shear capacity of the structure.

4.1 FE model

Figure 8 reports the mesh adopted with the PARC_CL model. Eight- node quadrilateral isoparametric plane stress elements based on quadratic interpolation and (3x3) Gauss integration have been adopted to describe the squat shear wall.

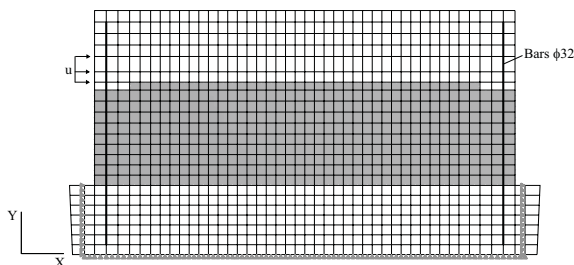


Figure 8: Adopted mesh for analyses with PARC_CL constitutive model.

Average concrete element dimensions of $100\text{mm} \times 100\text{mm}$ have been adopted in the mesh. The lateral $\phi 32$ bars are embedded in the flanges and they are free in the web. The

analyses have been carried out in displacement control using a regular Newton-Raphson convergence criterion based on force control with a tolerance of $5 \cdot 10^{-3}$ and 10^{-2} respectively in ABAQUS and DIANA.

4.2 Influence of the constitutive relations and interface mechanisms characterizing the transmission of shear forces

As well know, when a reinforced concrete structure is subjected to shear, different phenomena are involved in the transmission of the shear forces. These phenomena should be clearly taken into account in FE models. In order to underline this aspect, a preliminary set of analyses have been carried out with the PARC_CL model. First, only the mechanical contributions given by concrete and steel is taken into account (Analysis A). Afterwards the contribution of aggregate interlock (Analysis B) and tension stiffening (Analysis C) have been considered. The three analyses are compared in terms of load versus displacement curve in Figure 9.

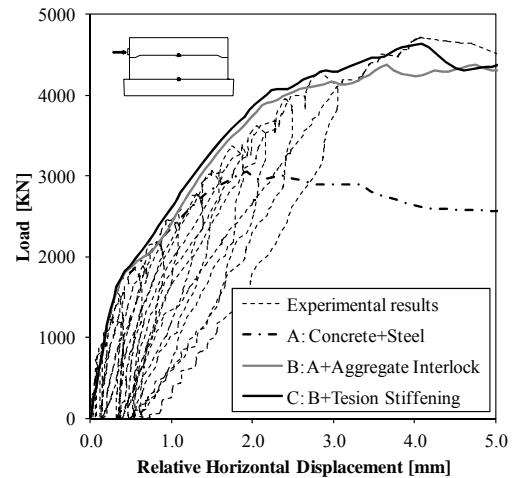


Figure 9: Comparison of the preliminary set of analyses carried out with PARC_CL model.

By considering only the mechanical contribution of concrete and steel (Analysis A), the shear capacity of the structure is underestimated, therefore the contributions given by the concrete-steel interaction phenomena play an important role.

By comparing analyses A and B, it is possible to note the large influence of the aggregate interlock. By comparing analysis B

to analysis C, it can be noted that the contribution due to the tension stiffening results not relevant in this case.

Analysis C gives the best prediction of the load versus displacement curve.

If the dowel action effect is taken into account in the model both the maximum load and the stiffness in the cracked phase are overestimated; for this reason the dowel action effect has been neglected in the study, in order, moreover, to be in the same conditions as DIANA model, in which the dowel action effect is not taken into account. However in future researches the authors will focus on the refinement of the dowel action modeling under loading-unloading-reloading conditions.

This preliminary study highlights the importance of a critic and adequate modeling of all the aspects involved in shear critical concrete structures [3][4].

Moreover, in the section 4.3 the results of Analysis C will be compared with the results obtained by the standard finite element code DIANA.

4.3 Comparison between NLFEA results

The same mesh, boundary conditions and convergence criterion have been adopted in PARC_CL and DIANA models.

In Figure 10 the comparison of the load-displacement curves is reported. The load-displacements curves of Figure 10 have been obtained using mean mechanical properties of materials.

For the analyses performed with DIANA both a total strain fixed and rotating crack models have been adopted. The analyses carried out with DIANA model, further explained in [9], have been carried out using the hypotheses listed below:

- total strain rotating and fixed crack model;
- variable Poisson's coefficient that linearly decreases from 0.19, in the elastic phase, up to 0.0 as the residual tensile stress is 0.0;
- maximum reduction of the compressive strength due to lateral cracking of 40% ($f_{c,red}/f_c=0.6$);
- tensile fracture energy G_f according to MC 2010 [10] ($G_{f,MC2010}=73f_c^{0.18}$);

- within the fixed crack model, variable shear retention factor that decreases from 1, in the elastic phase, up to 0.0 as Young's modulus and Poisson's coefficient reduce.

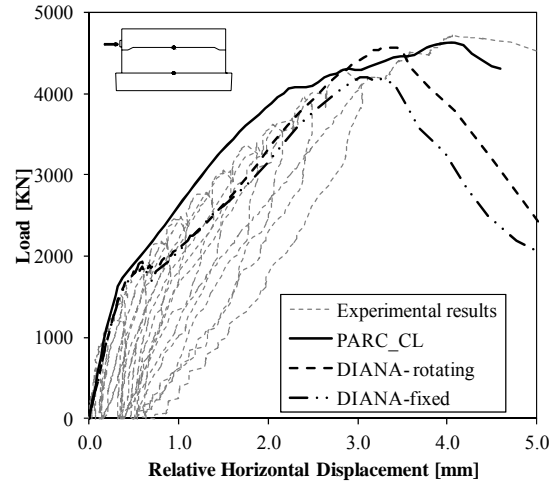


Figure 10: Load-displacement curves: comparison between PARC_CL and DIANA models.

From Figure 10 it can be noted that, within the standard code DIANA, there is a little difference between the fixed crack model and the rotating crack model both in the peak load and in the stiffness of the structure in the cracked phase.

The peak load is well predicted both with PARC_CL model and with the rotating crack model of DIANA. The greatest difference between the two models is again in the stiffness of the structure in the cracked phase and in the peak deformation.

As a matter of fact the stiffness of shear critical structures in the cracked phase is sensitively influenced by the concrete-to-concrete and concrete-to-reinforcement interface behavior, especially by the aggregate interlock effect (see Figure 9). Indeed the different modeling of the aggregate interlock effect in PARC_CL model (see section 3.2) and in DIANA model (where the shear retention factor decreases from 1, in the elastic phase, up to 0.0 as Young's modulus and Poisson's coefficient in the principal stress direction reduce) leads to some differences in the structural prediction.

Furthermore the difference detected between the two models is mostly in the stiffness of the structure and not in the shear capacity value

due to the high amount of steel reinforcement ($\rho_x=\rho_y=0.1\%$) of the structure. If structures without shear reinforcement would be analyzed with different crack models, the different refinement level of the aggregate interlock modeling would lead to a difference even in the shear capacity.

In Figure 11 the load-crack width curve of crack number 9, shown in Figure 11, is plotted.

In Figure 12 the crack pattern obtained for some significant load steps is plotted in terms of tensile cracking strain. The crack pattern obtained from NLFEA is compared to the experimental crack pattern, shown in Figure 12.

In Figure 13 the concrete compressive strain is plotted for some significant load steps.

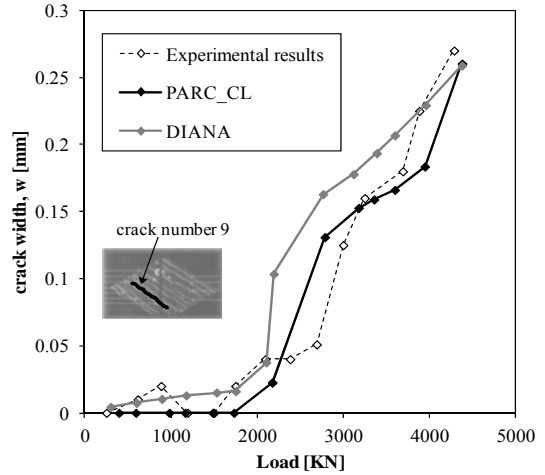


Figure 11: Load versus crack width curve.

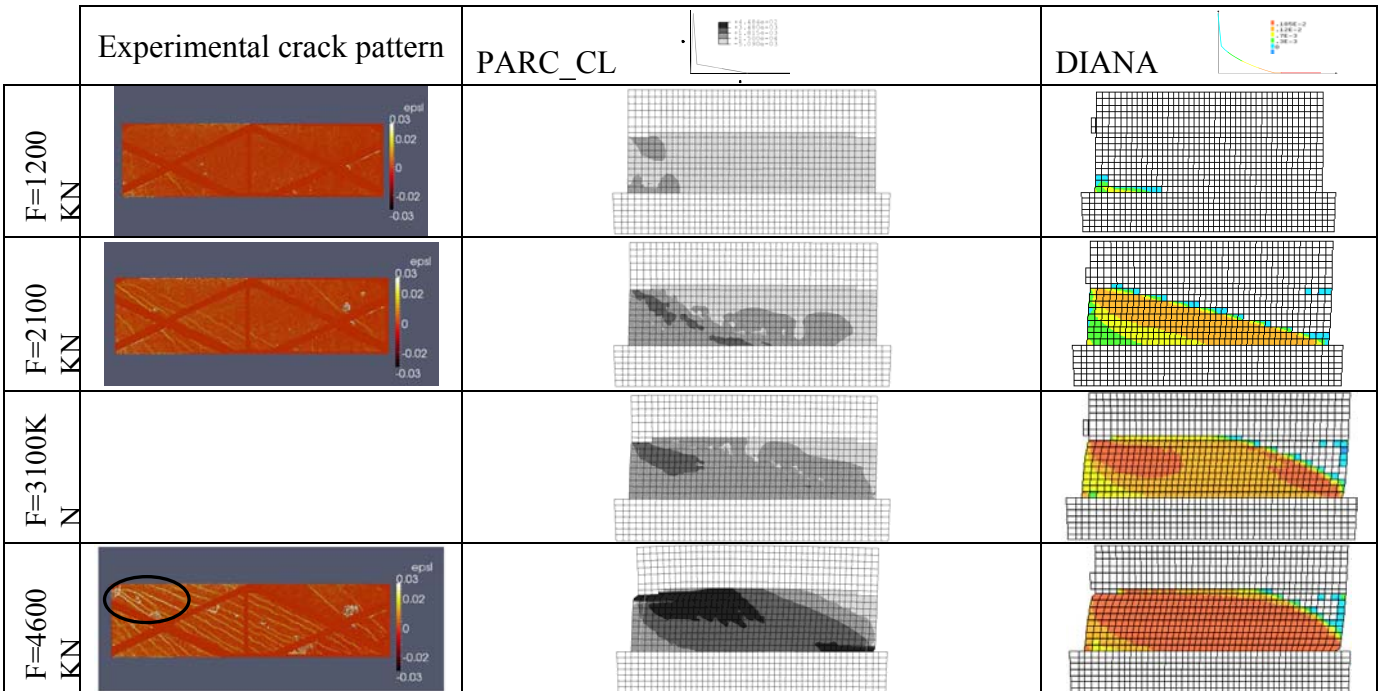


Figure 12: Comparison among the experimental and numerical results (PARC_CL and DIANA) in terms of crack pattern.

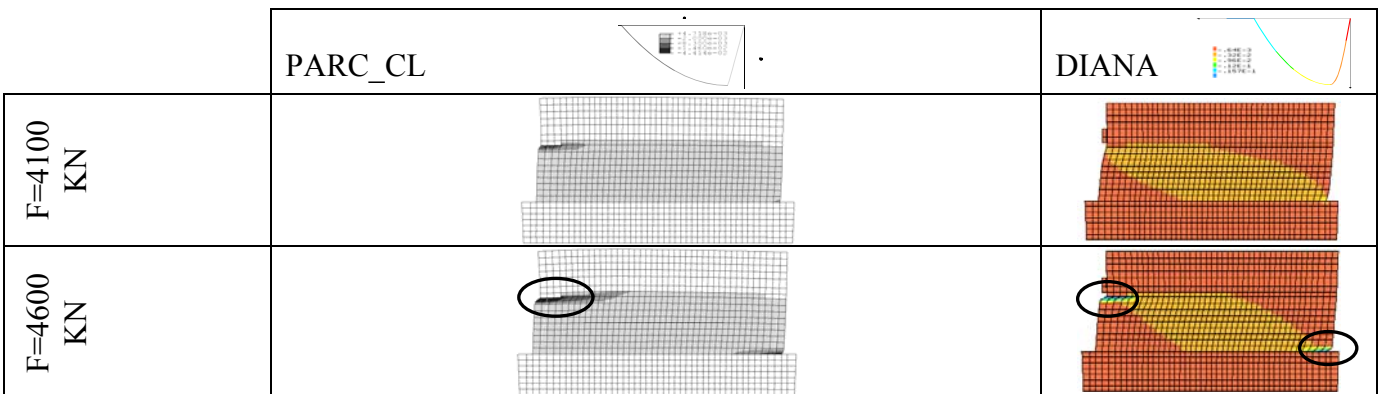


Figure 13: Comparison between numerical results (PARC_CL and DIANA) in terms of concrete compressive strain.

Table 2: Safety format methods.

	Input mechanical properties	Design shear capacity
GRF	mean	$P_d = \frac{P_{u,m}}{1.27}$
PF	design	$P_d = P_{u,d}$
ECOV	-characteristic -mean	$P_d = \frac{P_{u,m}}{1.06 \cdot \gamma_R}$ $\gamma_R = \exp\left(0.8 \cdot 3.8 \cdot \left[\frac{1}{1.65} \ln(P_{u,m}/P_{u,c})\right]\right)$

From Figure 12 and Figure 13 a good agreement among the results obtained with the two models in terms of crack pattern and failure mode is detected.

The same modeling used for the prediction of the structural behavior inputting mean mechanical properties of materials (Figure 10) has been adopted for the application of the safety format methods (Level IV) for the evaluation of the design shear carrying capacity.

According to the three safety format methods (GRF, PF, ECOV) different material properties are required in NLFEA as input data and the peak loads obtained from the analyses are reduced in order to obtain the same safety level as analytical procedures.

Table 2 summarizes the input mechanical properties required in the analyses and the calculation methods for the design shear capacity (P_d) evaluation, starting from the peak load obtained in the analyses (P_u).

5 EVALUATION OF THE DESIGN SHEAR CAPACITY WITH ANALYTICAL CALCULATION

In order to compare the design shear capacity obtained from NLFEA and the design shear capacity calculated analytically, the wall has also been analyzed with a strut and tie model, according to the prescriptions of MC2010 [10] and of [17].

For the squat shear wall analyzed in this paper the concrete strut runs from the loading plate to the bottom right corner of the web panel.

The design shear capacity P_d of a squat element can be in general determined as:

$$P_d = \sigma_{Rd,max} \cdot A_{str} \cdot \cos \theta \quad (27)$$

where θ is the strut inclination angle equal to 12° , $\sigma_{Rd,max}$ is the maximum compressive stress at the edge of the node (in the bottom right corner), evaluated, according to MC2010, as:

$$\sigma_{Rd,max} = \frac{k_c \cdot f_{ck}}{\gamma_c} = 16.46 \text{ MPa} \quad (28)$$

For compression-tension nodes with anchored ties provided in one or two directions k_c is determined as:

$$k_c = 0.75 \cdot \eta_{fc} = 0.716 \quad (29)$$

$$\eta_{fc} = \left(\frac{30}{f_{ck}}\right)^{1/3} = \left(\frac{30}{34.5}\right)^{1/3} = 0.954 \leq 1$$

A_{str} is the area of the concrete strut, Eq. (30):

$$A_{str} = t_w \cdot a_s = 0.15 \cdot 1.05 = 0.157 \text{ m}^2 \quad (30)$$

t_w is the web thickness and a_s is the width of the concrete strut. According to [17] the width of the concrete strut can be in a simplified way determined as:

$$a_s = \left(0.25 + 0.85 \frac{N}{A_c f_c}\right) \cdot l_w \quad (31)$$

$$= 0.25 \cdot 4.2 = 1.05 \text{ m}$$

where l_w is the wall length.

The design shear capacity of the wall obtained with the strut and tie model is therefore equal to $P_d=2536$ KN.

6 CONCLUSIONS AND FINAL DISCUSSION

In this paper the behavior of a squat shear wall subjected to monotonic loading is investigated. The wall has been analyzed with

NLFEA applying the constitutive model PARC_CL and the software DIANA. The results obtained with the two codes have been compared to the experimental results available from the experimental programme CEOS.fr. Furthermore the design shear capacity has been evaluated, with the two models, according to the calculation methods proposed by the MC 2010 (see section 4.3).

In Figure 14 the design shear capacity, P_d , obtained with analytical and numerical procedures proposed by the MC 2010 is expressed as a percentage of the experimental shear capacity, $P_{u, exp}$. The results obtained with DIANA plotted in Figure 14 refer to the fixed crack model, in order to be consistent with the results of PARC_CL model.

In Figure 15 the load-displacement curves obtained inputting characteristic and design mechanical properties of materials in PARC_CL and DIANA models are plotted.

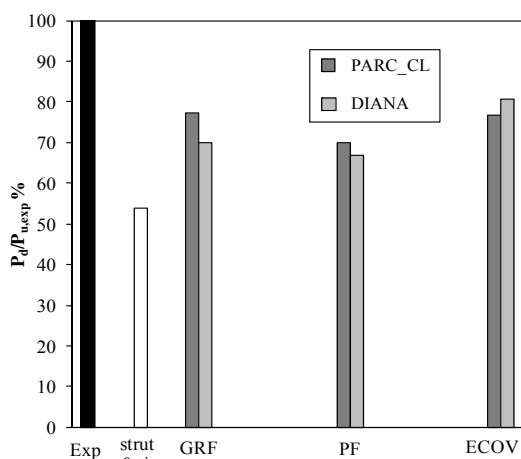


Figure 14: Design shear capacity P_d obtained analytically (strut and tie) and numerically (GRF, PF, ECOV [10]) with PARC_CL model and DIANA model, expressed as a percentage of the experimental shear capacity $P_{u,exp}$.

Figure 14 shows that in general the results obtained well match with the philosophy of the MC 2010 [10]: the design shear capacity obtained from NLFEA is higher than the design shear capacity obtained with simple analytical calculations (increase of 43%) for both PARC_CL and DIANA models. NLFEA represent in fact powerful instruments able to take into account for real material properties

and “hidden” capacities of the structure. This aspect can of course be of big help for both designers and researches in civil engineering, especially within intervention plans on existing structures.

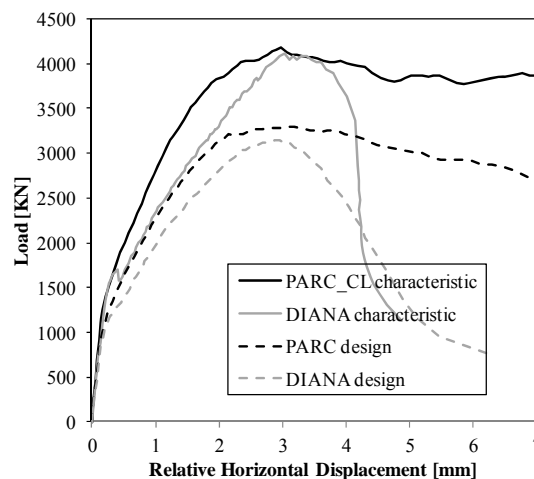


Figure 15: Load-displacement curves obtained with characteristic and design mechanical properties of materials with PARC_CL and DIANA models.

The design shear capacity obtained with PARC_CL model is higher than that one obtained with DIANA model with a scatter ranging from 2% to 9%. (ECOV method provided a higher shear capacity with DIANA model because of the ratio between the mean and characteristic peak loads (see Table 2)).

The same trend obtained and discussed in section 4.3 when mean mechanical properties of materials are inputted in NLFEA (see Figure 10) has also been obtained with characteristic and design mechanical properties, Figure 15: PARC_CL model provided greater stiffness in the cracked phase and slightly greater peak load values than DIANA model.

The difference in the results obtained could be due therefore, as anticipated, to some influencing aspects of the crack model implemented, like the aggregate interlock effect and the multi-axial stress state effect.

As a matter of fact in PARC_CL model the aggregate interlock directly depends on the compressive strength value (see eq.(12)-(17)), while in DIANA model the aggregate interlock effect is modeled in a rather simplified way: the shear retention factor in fact only decreases

with decreasing of the Young's modulus and the Poisson's coefficient in the principal stress directions.

Furthermore the reduction of the compressive strength due to lateral cracking is taken into account in DIANA model only by reducing the peak strength and not the peak strain, leading to a higher reduction of the structural stiffness, already in the elastic phase.

The aforementioned parameters of the crack model can in general affect the structural prediction, especially for shear critical structures, leading also to misinterpretation of the design shear carrying capacity. It is therefore important that designers well know the basis hypotheses of the crack models used or provide implementation of adequate laws of the nonlinear behavior of RC structures.

REFERENCES

- [1] French national research programme CEOS.fr: Behaviour and assessment of special construction works concerning cracking and shrinkage.
- [2] Rospars, C., Delapalce A., 2010. Synthesis results related to Squat shear wall. *2nd Workshop on Control of Cracking in R.C. Structures*, 20-22 June 2010, Paris, France.
- [3] Walraven, J.C., Belletti. B., Esposito, R. Shear Capacity of Normal, Lightweight & High-Strength Concrete beams according to MC2010. Part I. *Journal of Structural Engineering*, posted ahead of print 18 Sept 2012, doi:10.1061/(ASCE)ST.1943-541X.0000742, in press.
- [4] Belletti, B., Esposito, R., Walraven, J.C. Shear Capacity of Normal, Lightweight & High-Strength Concrete beams according to MC2010. Part II. *Journal of Structural Engineering*, posted ahead of print 18 Sept 2012, doi:10.1061/(ASCE)ST.1943-541X.0000743, in press.
- [5] ABAQUS, Analysis User's Manual, version 6.5, 2004.
- [6] Belletti, B., R. Cerioni, and I. Iori, *Physical approach for reinforced-concrete (PARC) membrane elements*. Journal of Structural Engineering, ASCE, 2001. **127**(12): 1412-1426.
- [7] Leonhardt, F., Schelling, G. 1974. Torsionsversuche an Stahlbetonbalken. Deutscher Ausschuss für Stahlbeton, D.A.f. St., *Heft 239, Ernest & Sohn*, Berlin.
- [8] Manie, J., 2009. DIANA user's manual. TNO DIANA BV.
- [9] Damoni, C., Belletti, B., Lilliu G. Control of cracking in R.C. structures: numerical simulation of a squat shear wall. *FraMCoS-8 Conference*, March 10-14, 2013, Toledo, Spain.
- [10] CEB-FIP Bullettins 65&66 - Model Code 2010 - Final Draft, International Federation for Structural Concrete (fib), Lausanne, Switzerland. 2012.
- [11] Feenstra, P.H., 1993. Computational Aspects of Biaxial Stress in Plain and Reinforced Concrete. PhD thesis, Delft Technische Universiteit Delft.
- [12] Nakamura, H. Higai, T., 2001. Compressive Fracture Energy and Fracture Zone Length of Concrete. *Benson P. Shing (editor)*, ASCE, pp. 471-487.
- [13] Vecchio, F.J., Collins, M.P., 1993. Compression response of cracked reinforced concrete. *Journal of Structural Engineering*, ASCE, **119** (12):3590-3610.
- [14] Gambarova, P.G., 1983. Sulla trasmissione del taglio in elementi bidimensionali piani di C.A. fessurati. *Proc., Giornate AICAP*, pp. 141-156.
- [15] Giuriani, E., 1981. On the effective axial stiffness of a bar in cracked concrete. *Bond in concrete*, P. Bartos, ed., Dept. of Civ. Engrg., College of Technology, Paisley, Scotland, pp 107-126.
- [16] Walraven, J.C., Reinhardt, H.W., 1981. Theory and experiments on the mechanical behaviour of cracks in plain and reinforced concrete subjected to shear loading. Heron, 26.
- [17] Paulay, T., Priestley, M. J. N., 1992. Seismic design of reinforced concrete and masonry buildings. *Wiley, New York*.